Original Investigation

Performance of Diffusion Kurtosis Imaging Versus Diffusion Tensor Imaging in Discriminating Between Benign Tissue, Low and High Gleason Grade Prostate Cancer

Maria Giovanna Di Trani, MSc, Marco Nezzo, MD, Alessandra S. Caporale, PhD, Riccardo De Feo, MSc, Roberto Miano, MD, Alessandro Mauriello, MD, Pierluigi Bove, MD, Guglielmo Manenti, MD, Silvia Capuani, PhD

Abbreviations

PCa prostate adenocarcinoma

DWI diffusion-weighted imaging

DTI diffusion tensor imaging

DKI diffusion kurtosis imaging

K apparent kurtosis

D apparent diffusivity derived from K

KFA proxy kurtosis fractional anisotropy

MD mean diffusivity

FA fractional anisotropy

GG Gleason grade

PT peritumoral tissue

Rationale and Objectives: To investigate the performance of diffusion kurtosis imaging (DKI) and diffusion tensor imaging (DTI) in discriminating benign tissue, low- and high-grade prostate adenocarcinoma (PCa).

Materials and Methods: Forty-eight patients with biopsy-proven PCa of different Gleason grade (GG), who provided written informed consent, were enrolled. All subjects underwent 3T DWI examinations by using *b* values 0, 500, 1000, 1500, 2000, and 2500 s/mm^2 and six gradient directions. Mean diffusivity, fractional anisotropy (FA), apparent kurtosis (K), apparent kurtosis-derived diffusivity (D), and proxy fractional kurtosis anisotropy (KFA) maps were obtained. Regions of interest were selected in PCa, in the contralateral benign zone, and in the peritumoral area. Histogram analysis was performed by measuring mean, 10th, 25th, and 90th (p90) percentile of the whole-lesion volume. Kruskal–Wallis test with Bonferroni correction was used to assess significant differences between different regions of interest. The correlation between diffusion metrics and GG and between DKI and DTI parameters was evaluated with Pearson's test. ROC curve analysis was carried out to analyze the ability of histogram variables to differentiate low- and high-GG PCa.

Results: All metrics significantly discriminated PCa from benign and from peritumoral tissue (except for K, KFA_{p90}, and FA). K_{p90} showed the highest correlation with GG and the best diagnostic ability (area under the curve = 0.84) in discriminating low- from high-risk PCa.

Conclusion: Compared to DTI, DKI provides complementary and additional information about prostate cancer tissue, resulting more sensitive to PCa-derived modifications and more accurate in discriminating low- and high-risk PCa.

Key Words: Diffusion kurtosis imaging; Low- and high-risk prostate cancer; DTI; Gleason grade; Histogram analysis.

Acad Radiol 2018; ■:1–10

From the Centro Fermi – Museo Storico della Fisica e Centro Studi e Ricerche Enrico Fermi, Rome, Italy (M.G.D.T., R.D.F.); Department of Anatomical, Histological, Forensic and Locomotor System Science, Sapienza University of Rome, Via A. Scarpa 16, Rome 00161, Italy (M.G.D.T.); Department of Diagnostic and Interventional Radiology, Molecular Imaging and Radiotherapy, PTV Foundation, Tor Vergata University of Rome, Rome, Italy (M.N., G.M.); Department of Physics, CNR ISC, UOS Roma Sapienza, Sapienza University of Rome, Rome, Italy (A.S.C., R.D.F., S.C.); Department of Radiology, University of Pennsylvania Hospital, Founders Pavilion, Philadelphia, Pennsylvania (A.S.C.); Urology Unit, Department of Experimental Medicine and Surgery, PTV Foundation, Tor Vergata University of Rome, Rome, Italy (R.M., P.B.); Anatomic Pathology, Department of Experimental Medicine and Surgery, PTV Foundation, Tor Vergata University of Rome, Rome, Italy (A.M.). Received October 9, 2018; revised November 19, 2018; accepted November 21, 2018. **Address correspondence to:** M.G.D.T. e-mail: mgiovanna.ditrani@gmail.com

https://doi.org/10.1016/j.acra.2018.11.015

GS
Gleason score

m
mean

p10
10th percentile

p25
25th percentile

p90
90th percentile

INTRODUCTION

Prostate adenocarcinoma (PCa) is the second most common malignancy and the fifth leading cause of death among men worldwide (1). Nowadays, the diagnostic power of diffusion-weighted imaging (DWI) and diffusion tensor imaging (DTI) metrics in PCa investigations has been largely demonstrated (2–8). However, the high incidence of PCa and the limitations of the current diagnostic tools (9) indicate that the development of more sensitive and specific techniques for the diagnosis and staging of PCa is highly desirable. In particular, an accurate differentiation between low-risk and intermediate/high-risk cancer is mandatory to ensure an appropriate management of patients, which can even include focal therapies or active surveillance (10–13).

DWI and DTI techniques exploit the physiologic movement of water molecules in biologic systems to reveal unique information of tissues architecture. Water diffusion in biologic tissues is confined by membranes, molecular crowding, and microstructures that impede and hinder water motion. Poorly interacting water molecules are characterized by faster dynamics, detected by using b values up to 1000 s/mm^2, where the b value represents the diffusion weight through which different diffusion dynamics can be selected. On the other hand, water molecules highly interacting with tissue microstructures are characterized by slower dynamics that can be measured using high b values, ie, b values higher than 1000 s/mm^2.

Prostate gland consists of a strongly heterogeneous tissue, where water experiences highly restricted diffusion in the approximately 15-μm thick epithelial cell layer, moderately restricted diffusion in the fibromuscular stroma and relatively free diffusion in the gland lumen and ducts (14,15). Generally, PCa changes the microstructural arrangement of these compartments, by increasing cell density and modifying the shape of glands and the integrity of membranes. These modifications affect water molecular motion, making DW-signal sensitive to tumor development.

Recently, it has been highlighted (16) that to increase the sensitivity and the specificity of diffusion parameters, it is necessary to employ high b values to quantify diffusion of biologic water that most interacts with cell membranes and tissue microstructures.

Diffusion kurtosis imaging (DKI) (17–20) technique provides a representation of Nuclear Magnetic Resonance (NMR) signal when high b values are employed and may offer a more detailed characterization of tissue microstructures. Hence, this work investigated whether DKI is more sensitive than DTI to tissue micromodifications caused by PCa, providing a more accurate diagnostic tool in PCa treatment.

DKI is a technique suitable for any biologic tissue, since it does not require a priori knowledge of tissue biophysical properties; rather, DKI is a representation of NMR signal when diffusion is probed with high b values. In particular, kurtosis is the fourth order term of DWI-signal expansion in terms of b value. This term is null in the case of free diffusion and quantifies diffusion heterogeneity arising from multiple tissue compartments with different diffusion behaviors (17).

In the last few years, some authors evaluated DKI performances in PCa diagnosis, referring an enhanced diagnostic power than DTI or ADC (21–24) and, in few cases, no significant benefit (25,26). However, in some works (21,27), the evaluation of signal-to-noise ratio (SNR) was missing and noise correction was not included in the processing of data, limiting the reliability of the derived parameters.

In order to test the ameliorated sensitivity and diagnostic specificity provided by DKI with respect to DTI, good quality images should be considered. For this reason, in this study, noise and Gibbs' ringing artifacts corrections were employed to process raw data and a new DKI-derived parameter was calculated, proxy kurtosis fractional anisotropy (KFA).

Therefore, the aim of this work was to investigate the diagnostic ability of DKI parameters, apparent kurtosis (K), kurtosis-derived apparent diffusivity (D) and KFA, in comparison to DTI parameters, mean diffusivity (MD), and fractional anisotropy (FA) in PCa detection and grading, using good quality images. Since malignant tissue could be interspersed within benign tissue, the performances of DKI and DTI metrics in differentiating benign tissue and Gleason grades (GG) (28,29) were evaluated by using histogram analysis of the entire volume lesion (21,22). Differences between diffusion parameters measured in PCa, benign, and peritumoral (PT) tissue were analyzed.

To evaluate and compare the potential of DKI and DTI parameters as markers of tumor aggressiveness, the correlation between diffusion metrics and Gleason grade (GG) was

evaluated by means of Pearson's test. In addition, Pearson's test was used to assess the independence of the information provided by DKI and DTI metrics on prostate tissue.

Finally, the diagnostic accuracy of DKI and DTI in discriminating low- from high-GG PCa was evaluated by ROC curve analysis.

MATERIALS AND METHODS

This study retrospectively included 48 patients with biopsy-proven prostate cancer. All subjects (Table 1) underwent the magnetic resonance imaging (MRI) examination between February 2015 and March 2016, providing informed consent. The targeted MR/ultrasound fusion biopsy (BiopSee, Medcom, Darmstadt, Germany) revealed lesions with Gleason score (GS) varying from 6 (ie, 3 + 3) to 9 (ie, 5 + 4) among the patients cohort. In this work, tumors were graded according to the system recently proposed by the International Society of Urological Pathology (ISUP) (28,29), which was proven to be more accurate in predicting PCa progression and in reflecting PCa biology. The ISUP grading system consists of five distinct GG, related to the GS as follows: GG1 = GS6, GG2 = GS3 + 4 = GS7, GG3 = GS4 + 3 = GS7, GG4 = GS4 + 4 = GS8, GG5 = GS9 and GS10.

Since several studies showed that GS4 + 3 demonstrates worse pathological stage and biochemical recurrence rates than GS3 + 4 (30,31), we consider GG $\leq$2 (GS $\leq$3 + 4) and GG $\geq$3 (GS $\geq$4 + 3) as low- and high-risk prostate cancer, respectively.

MRI Acquisition

The MRI experiments were performed using a 3 T clinical scanner (Intera Achieva, Philips Medical Systems, the Netherlands) equipped with a maximum gradient strength of 80 mT/m and a slew rate of 200 mT/m/ms. A six-channel phased array SENSE torso coil was used in all the examinations. The acquisition protocol included high spatial resolution T2-weighted turbo spin echo and DWI with echo-planar imaging. T2-weighted turbo spin echo images (repetition time = 3957 ms, echo time = 150 ms, turbo factor = 21, field of view = 150 × 130 mm^2, slice thickness = 3 mm, gap = 0, acquisition matrix = 256 × 178, reconstruction matrix = 512 × 512, number of averaged scans = 2, flip angle = 90°) were acquired for all subjects including the entire gland in the axial plane. DWI protocol was carried out both for DTI and DKI with a single-shot echo-planar imaging sequence (repetition time = 3000 ms, echo time = 67 ms, field of view = 150 × 130 mm^2, acquisition matrix = 64 × 52, reconstruction matrix 96 × 96, slice thickness = 3 mm, gap = 0, number of averaged scans = 4), by using six b values (0, 500, 1000, 1500, 2000, 2500 s/mm^2) and six no-coplanar gradient diffusion directions. Spectral attenuated inversion recovery fat suppression with 200 Hz frequency offset was used after a B_0 homogeneity optimization by using high-order shim routine. The acquisition time of the entire protocol was approximately 12 minutes, nine of which used for the diffusion protocol. T2-weighted images (T2WIs) were employed as anatomical and morphological reference to determine region of interests (ROIs).

Biopsy

All patients underwent biopsy in a period of 1 day—2 weeks after the MRI examination by expert urologists. T2WIs were used to contour and record lesion locations (Watson Elementary). Targeted MR/ultrasound fusion biopsy (BiopSee, Medcom, Darmstadt, Germany) was performed by taking from 2 to 4 biopsy cores from the targets, followed in the same session by a 12-core transperineal biopsy (sextant and laterally directed biopsies at base, midgland, and apex). The standard 12-core transperineal biopsy was performed by a different physician, who was unaware of the MR findings. For each specimen, histopathological examination was performed and reviewed following the recommendations of the "consensus conference ISUP 2014" (29).

According to the ethics committee regulations of our country, this work did not need the Institutional Review Board (IRB) approval, since it was a retrospective study and it was conducted by ensuring anonymity and confidentiality of the data.

All patients underwent MRI scan and biopsy regardless of this study, according to the standard urogenital radiology clinical routine, following the European Society of Urogenital Radiology guidelines.

Data Preprocessing

All DWIs were corrected for motion artifacts by using FLIRT, a tool of FSL 5.0 software: each volume was registered to b0-image through a rigid-body transformation with three degrees of freedom (32).

Volumetric ROIs (Fig 1) were selected in the entire prostate gland, in PCa area, in PT region and in benign tissue. The benign ROI was selected in correspondence to the

TABLE 1. Patients' Cohort

GG	1	2	3	4	5	Total
GS	3 + 3	3 + 4	4 + 3	4 + 4	4 + 5; 5 + 4	
No. of patients	16	14	8	6	4	48
No. of slices	25	22	15	16	13	91
Patients' age	72 (57–88)	74 (62–79)	66 (50–73)	63 (69–82)	76 (53–73)	72 (50–88)

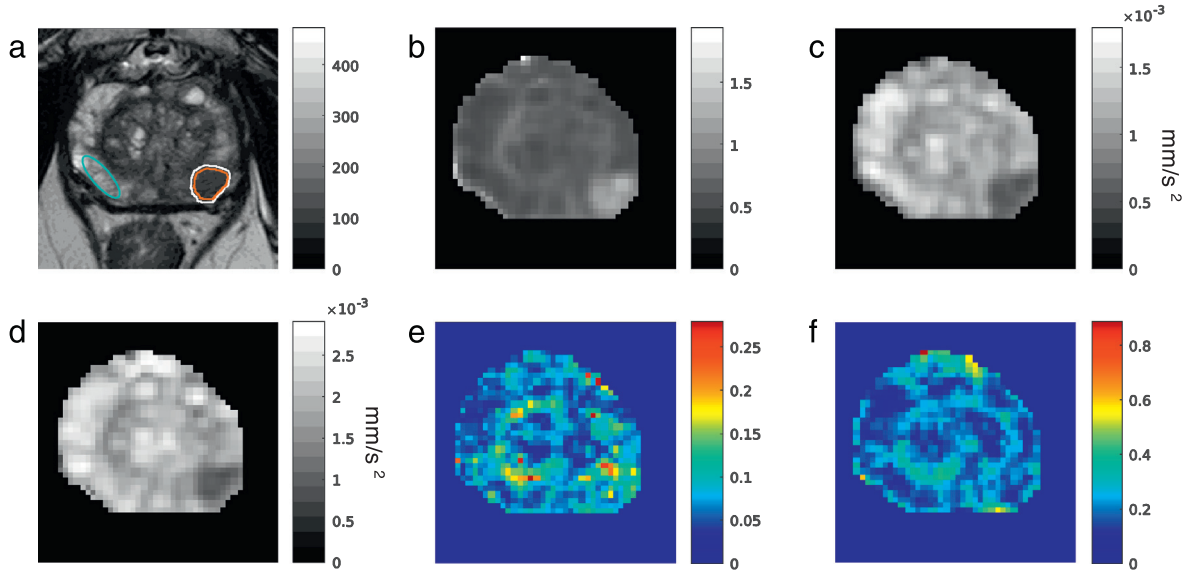

Figure 1. Diffusion parametric maps. T2-weighted image (**a**) with outlined PCa (orange), PT (white), and benign ROIs (light blue). The presence and the extension of malignant tissue (subject with a GG3 lesion) is clearly visible in K-, MD-, and D map (**b, c**, and **d**, respectively). FA map (**f**) shows no contrast between PCa and benign tissue, while in KFA map (**e**) PCa appears slightly more intense than benign tissue; however, it is not sufficient to correctly individuate PCa region or PCa extension. (Color version of figure is available online.)

PCa-ROI, but in the contralateral lobe. PT regions were considered as the nearest pixels to the PCa-ROI edge. All ROIs (144 in total, including 48 lesions, 48 contralateral control regions, and 48 PT regions) were manually drawn on the MD maps by referring to T2WIs, with particular care to avoid calcification, necrosis, and neurovascular bundles.

Data Analysis

The conventional DTI analysis was carried out by DTIFIT routine of FSL with a *b*-value range (0−1000 s/mm^2) (32,33); MD and FA were calculated from the diffusion tensor eigenvalues as follows (34):

$$\mathrm{MD} = \frac{\lambda_1 + \lambda_2 + \lambda_3}{3};$$

$$\mathrm{FA} = \sqrt{\frac{3}{2}} \cdot \frac{(\lambda_1 - \mathrm{MD})^2 + (\lambda_2 - \mathrm{MD})^2 + (\lambda_3 - \mathrm{MD})^2}{\lambda_1^2 + \lambda_2^2 + \lambda_3^2} \quad (1)$$

DKI metrics were obtained by fitting DWI signal up to 2500 s/mm^2 along each direction to the equation (33,35):

$$\ln\left(\frac{S(n)}{S_0}\right) = -b\mathrm{D}(n) + \frac{1}{6}b^2\mathrm{D}(n)^2 \cdot \mathrm{K}(n) \quad (2)$$

where K(n) is the kurtosis and D(n) the relative apparent diffusion coefficient, both estimated in a given diffusion direction n.

In this manner, we estimated K(n) and D(n) for each encoding direction; then, maps of mean apparent kurtosis (K) and mean apparent diffusion coefficient (D) were calculated by averaging over the six diffusion gradient directions, as follows:

$$\mathrm{K} = \frac{1}{6}\sum_{i=1}^{6}\mathrm{K}(n_i); \quad \mathrm{D} = \frac{1}{6}\sum_{i=1}^{6}\mathrm{D}(n_i) \quad (3)$$

With the DWI protocol used in this study, the kurtosis tensor, whose estimate requires at least 15 gradient directions (17), could not be calculated; therefore, we estimated an apparent kurtosis.

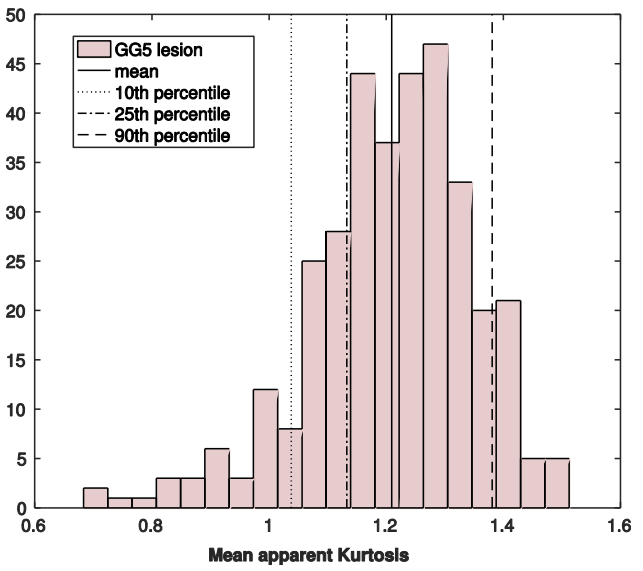

Figure 2. Histogram metrics. The histogram-derived metrics (mean, 10th, 25th, and 90th percentile) were pointed out in the histogram of K, measured in the entire PCa-ROI of a representative subject with a GG5 lesion.

The fitting procedure, developed in Matlab (MATLAB R2016b, The Mathworks, Natick, Massachusetts), performed a voxel-by-voxel nonlinear least-squares analysis, using a trust-region-reflective algorithm.

Moreover, parametric maps of proxy KFA were calculated as proposed by Hansen and Jespersen (36):

$$\mathrm{KFA} = \frac{\mathrm{SD}(\mathrm{K}(n))}{\mathrm{RMS}(\mathrm{K}(n))} \quad (4)$$

where SD indicates the standard deviation, RMS the root-mean-square value, and n the diffusion gradient directions.

Parametric maps of DKI and DTI metrics were obtained for the entire cohort of patients.

Since cancer tissue could include normal tissue, calculating the mean of diffusion parameters in ROIs may not be the best quantification of diffusion metrics in PCa. For this reason, we performed histogram analysis (37), by measuring, in addition to the mean (m) and the standard deviation (SD), the 10th (p10), 25th (p25), and 90th (p90) percentile of the distribution, ie, the histogram, of diffusion parameters measured in volumetric ROIs. The percentile of a distribution indicates the value below which a given percentage of observations falls: in our case, the 10th, 25th, and 90th percentiles represent the values below which the 10%, 25%, and 90% of the measures lie, as indicated in Figure 2.

Finally, SNR was calculated in both PCa and normal tissue, considering the internal obturator muscle as background signal, as follows:

$$\mathrm{SNR} = \frac{\mathrm{mean(signal)}}{\mathrm{SD(background\ signal)}} \quad (5)$$

Statistical Analysis

Kruskal–Wallis test with Bonferroni correction (38) was carried out to assess statistical significance of differences in each diffusion parameter between PCa, benign, and PT tissue. The correlation between diffusion parameters and GG and the cross-correlations between DTI and DKI metrics in benign, low-, and high-GG tissues were assessed with Pearson's correlation test.

Finally, the ROC curve analysis was carried out to investigate the diagnostic ability of each diffusion parameter in distinguishing low- and high-grade tumors. The best cut-off value was evaluated as the value that maximizes the Youden index (sensitivity + specificity − 1).

A $p \leq 0.05$ was considered as statistically significant.

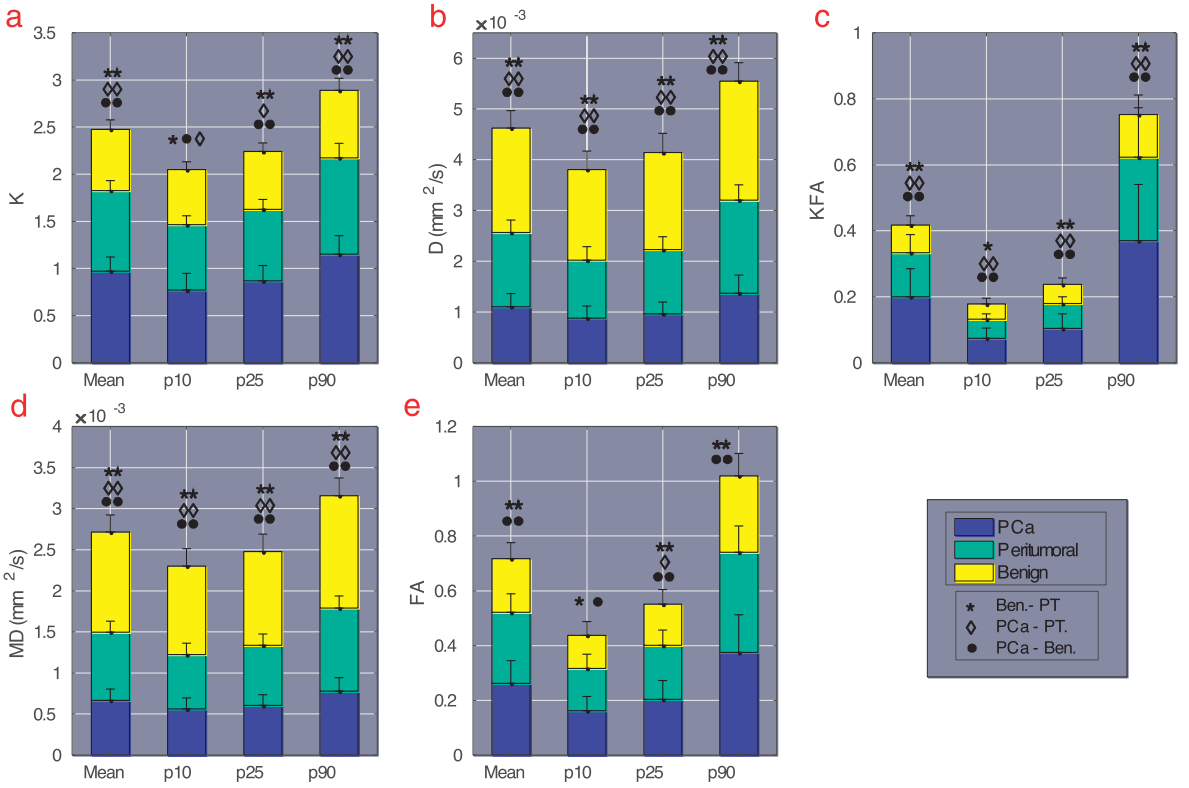

Figure 3. Diffusion measures in PCa, PT, and benign regions. *Stacked bargraphs* show mean and SD of histogram metrics calculated in PCa (*blue bars*), PT (*light green bars*), and benign (*yellow bars*) tissue for each diffusion parameter: kurtosis (**a**), mean diffusivity (**b**), K-derived diffusion coefficient D (**c**), kurtosis fractional anisotropy (**d**), and fractional anisotropy (**e**). Symbols indicate the p value of Kruskal–Wallis test performed between PT and benign (*), PCa and PT (◊), and PCa and benign tissue (•). * $p < 0.05$; ** $p < 0.001$. (Color version of figure is available online.)

TABLE 2. Pearson's Coefficient *r* and *p* Value of the Correlation Between Histogram Metrics of Diffusion Parameters and GG

		Mean	10th percentile	25th percentile	90th percentile
K	*r*	0.51	0.30	0.42	0.52
	p value	0.001	0.072	0.009	0.001
D	*r*	−0.27	−0.36	−0.29	−0.22
	p value	0.106	0.028	0.076	0.189
KFA	*r*	−0.20	−0.23	−0.26	−0.13
	p value	0.222	0.158	0.114	0.445
MD	*r*	−0.36	−0.41	−0.39	−0.27
	p value	0.028	0.011	0.017	0.102
FA	*r*	0.16	−0.01	0.06	0.20
	p value	0.333	0.968	0.738	0.242

RESULTS

SNR was higher than 10 for all subjects at the highest *b* value = 2500 s/mm^2, both for PCa and benign prostatic regions.

Statistically significant differences were found between PCa and benign tissue for DTI (MD and FA) and DKI parameters (K, D, and KFA) with $p < 10^{-3}$.

PT tissue was significantly different from PCa tissue (except for K, KFA_{p90}, and FA) and from benign tissue for all parameters (Fig 3).

K-histogram-derived parameters exhibited a stronger positive correlation with tumor grade ($r_m = 0.51$, $r_{p25} = 0.42$, $r_{p90} = 0.52$, $p < 0.009$, Table 2), except for the 10th percentile. Among histogram metrics of D, only the 10th percentile was weakly correlated with GG ($r_{p10} = -0.36$, $p < 0.03$). The mean, 10th, and 25th percentile of MD showed a weak negative correlation with GG ($r_m = -0.36$, $r_{p10} = -0.41$, $r_{p25} = -0.39$, $p < 0.05$).

No significant correlations were found between the remaining diffusion parameters (KFA and FA), their histogram-derived measures, and the tumor grade (Table 2).

Except for FA and KFA, diffusion maps showed a good contrast between PCa and benign tissue (Fig 1). The ROC curve analysis (Table 3) suggested that K_{p90} has the best diagnostic ability, ie, the higher area under the curve (AUC) in distinguishing low- from high-grade PCa (AUC = 0.84), followed by MD_{p10} (AUC = 0.72), D_{p10} (AUC = 0.67), KFA_{p25} (AUC = 0.67; Table 3 and Fig 4). Histogram metrics of FA showed a performance similar to a random classifier with the maximum AUC = 0.55 for FA_m.

Histograms of diffusion metrics of one patient with GG1 and one patient with GG4, randomly chosen, are showed in Figure 5.

Scatterplots in Figure 6 pointed out the relation between DKI and DTI parameters, while the results of their correlation (Pearson's test) are reported in Table 4.

TABLE 3. ROC Curve Analysis Results Obtained for Histogram Metrics of Each Diffusion Parameter

		K	D	KFA	MD	FA
Mean	AUC	0.79	0.62	0.61	0.69	0.55
	Sp	77.8	100	51.9	85.2	44.4
	Se	81.8	27.3	72.7	45.5	72.7
	Cut	1.03	0.82*	0.26	0.73*	0.24
10th percentile	AUC	0.69	0.67	0.66	0.72	0.50
	Sp	51.9	100	51.9	85.2	48.1
	Se	90.9	36.4	81.8	54.5	72.7
	Cut	0.67	0.63*	0.09	0.59*	0.17
25th percentile	AUC	0.74	0.64	0.67	0.71	0.50
	Sp	74.1	100	59.3	85.2	22.2
	Se	72.7	27.3	72.7	54.5	90.9
	Cut	0.90	0.73*	0.11	0.63*	0.16
90th percentile	AUC	0.84	0.63	0.59	0.65	0.51
	Sp	88.9	77.8	55.6	85.2	85.2
	Se	72.7	54.5	72.7	45.5	27.3
	Cut	1.28	1.18*	0.50	0.86*	0.54

Area under the curve (AUC), specificity (Sp), sensitivity (Se), and cut-off (Cut) values are reported.

* ($\times 10^{-3}$ mm^2/s).

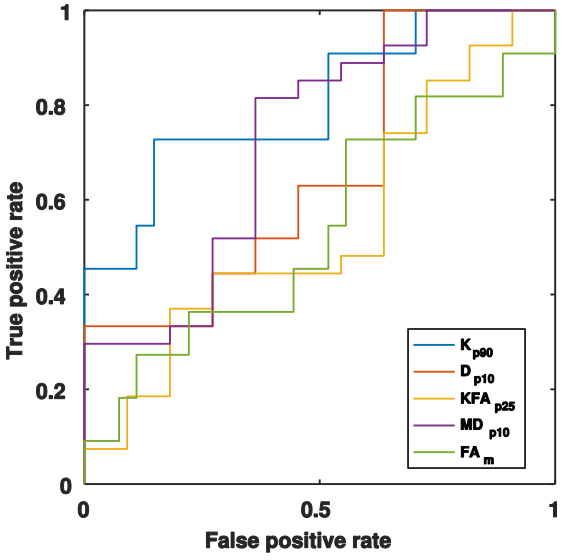

Figure 4. ROC curves. ROC curves reflect the diagnostic potential in discriminating low- from high-GG prostate cancer of DKI and DTI parameters that produced the highest AUC. K_{p90} showed the best AUC and, along with MD_{p10}, an evident better performance than D, KFA, and FA.

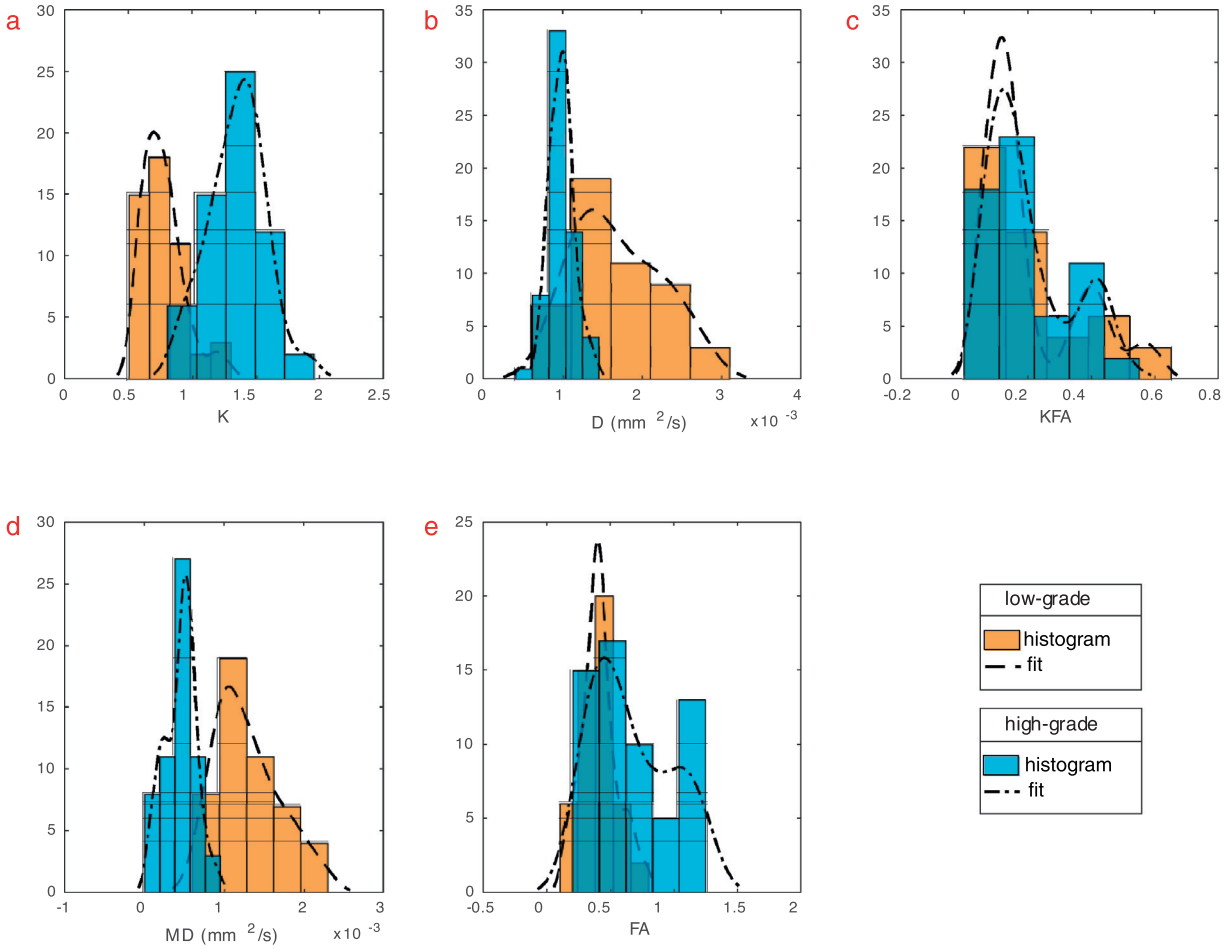

Figure 5. Histograms of low- and high-GG prostate tissue. Distribution of DKI and DTI parameters of two subjects, randomly chosen, representing low- and high-GG prostate tissue (GG1 and GG4, respectively). K histograms exhibited the best separation between low- and high-risk PCa (**a**). MD- and D histograms (**d** and **b**) show a good separation between tumor grades, while KFA- and FA histograms (**c** and **e**) show a strong overlap.

DISCUSSION

In this study, we investigated the performance of DKI compared to DTI in PCa grading, using the ISUP grading system (28,29).

Since low SNR can bias diffusion parameters estimation, to validate the reliability of the quantified metrics, we calculated the SNR of DWIs as a function of b values. We found that the SNR was higher than 10 for $b = 2500$ s/mm^2 for each patient, a value well above the critical value SNR = 3 (39).

Our estimation of DKI parameters in benign and cancerous prostate tissue was in general accordance with other studies, that referred SNR 29.3 ± 9.9 (23) and 34.81 ± 6.44 (24) (both calculated at $b = 2000$ s/mm^2), comparable to the mean values calculated in this study, where SNR was 18.02 ± 7.4 (calculated at $b = 2500$ s/mm^2) in PCa region.

In literature, the outcomes of DKI in PCa diagnosis are discordant, including studies that found an increased value for DKI in PCa assessment (21–24) and studies that found no significant advantages in using DKI for PCa detection and grading (25,26).

In our work, K showed a superior diagnostic power in discriminating low- and high-grade PCa. This is probably because, unlike previous studies that used three diffusion gradient directions, we have evaluated K using six gradient directions and we used a different classification of tumor grades (28,29) with a different definition of low- and high−risk PCa.

Results of this study showed that DTI and DKI with entire-lesion histogram analysis enable to discriminate patients with PCa of different aggressiveness grades. In agreement with Wang et al. (21), K_{p90} showed the strongest correlation with GG and the best diagnostic ability in differentiating high- from low-grade PCa, according to the ROC analysis.

MD histogram metrics showed good performance in correlating with GG and in differentiating low- and high-risk patients; however, K metrics showed a stronger correlation with GG and the highest AUC.

By examining histograms of low- and high-grade tissues (Fig 5), it is evident that K showed the largest separation.

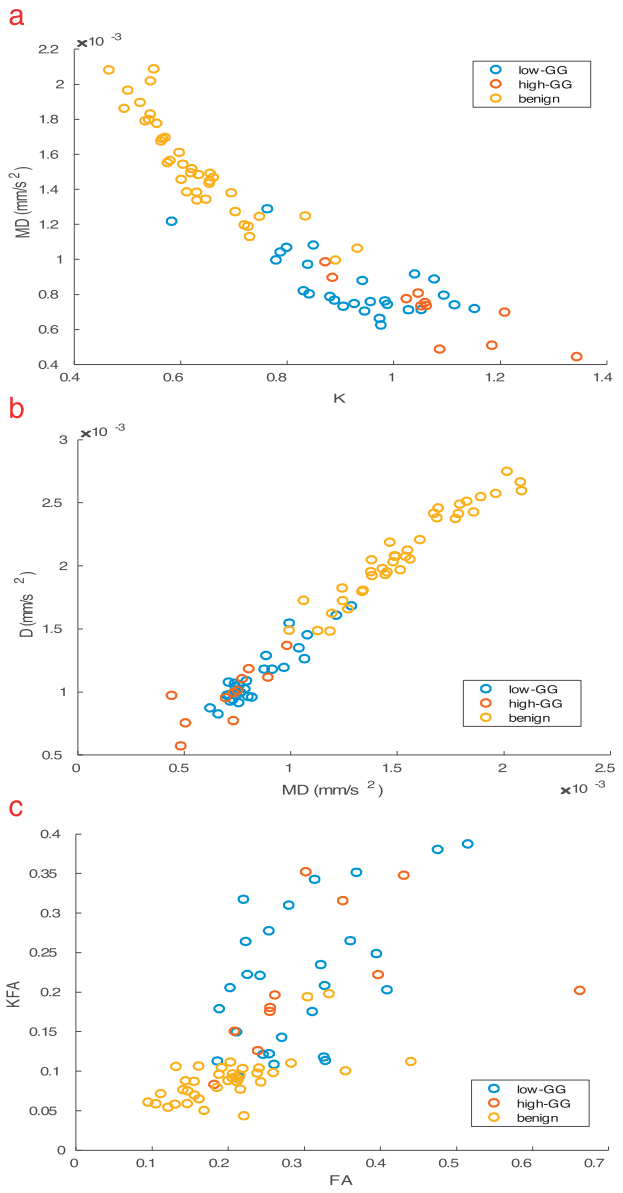

Figure 6. Correlations between DTI and DKI metrics. Correlations between DTI and DKI parameters measured in benign (yellow), low (blue), and high (orange) GG prostate tissue. As expected, D and MD are highly correlated (**b**). K and MD show a general inverse correlation (**a**), weaker for low-GG PCa, suggesting that DTI and DKI metrics provide complementary information on investigated tissue. Except for benign and low-GG tissue, where they are moderately correlated, KFA and FA are uncorrelated (**c**) in high-GG PCa and their behavior in prostate tissue should be clarified. (Color version of figure is available online.)

Besides, K histogram was broader in high-grade than in low-grade tissue. This may be due to the peculiar structural heterogeneity of high-grade PCa characterized by great irregularity of glands shape and arrangement.

Conversely, the high variability of MD and D in low-grade cancer tissue (broader histograms) may reflect the presence of several diffusion compartments characterized by fast and hindered diffusion dynamics that tend to vanish when glandular structure is disrupted by high-grade cancer, resulting in distributions peaked at low diffusion values for PCa regions.

TABLE 4. Pearson's Test Results of the Correlation Between DTI and DKI Parameters

		Low GG	High GG	Benign
K vs MD	*r*	−0.71	−0.85	−0.89
	p value	$<10^{-4}$	$<10^{-2}$	$<10^{-4}$
D vs MD	*r*	0.93	0.79	0.96
	p value	0.002	0.004	$<10^{-4}$
KFA vs FA	*R*	0.54	0.27	0.62
	p value	0.034	0.210	$<10^{-4}$

Other than the cancer, the surrounding region of PCa lesion (PT) may provide cues on the prognosis and aggressiveness of the lesion itself. For example, mast cells in PT region promote angiogenesis and can be prognostic markers in prostate cancer (40); moreover, the PT lymphatic vessel density varies with the GS and with the presence of regional lymph node metastases (41). Therefore, a precise evaluation of PT region may increase the accuracy in the definition of tumor extension, and potentially provide indications about future developments of the lesion. In this work, we tested the sensitivity of diffusion parameters with respect to the PT tissue, finding a statistically significant difference between the PT region and both PCa and benign tissue, suggesting diffusion properties of this transitional zone distinct from both the benign and cancer tissues.

As indicated by their strong correlation (Fig 6b), MD and D reflected the properties of prostate tissue similarly. In fact, according to previous studies (21−24), we found MD and D to be lower in cancer tissue, because of infiltrating malignant cells restricting water molecular motion. Conversely, K assumed higher values in PCa, revealing the increased complexity and heterogeneity of tumor histoarchitecture.

The variations of tissue diffusion properties are strictly related to the morphological modifications caused by PCa: glands change in size and shape and malignant cells infiltrate ducts and acini, reducing the free available space for molecular motion (42). The general inverse correlation between K and MD (Fig 6a) pointed out how the overall effect of these micromodifications is a combination of reduced diffusivity and increased tissue heterogeneity. However, in low-grade PCa lesions (GG2, blue data points in Fig 6a), the correlation between K and MD was weaker than in benign and high-GG (Table 4). In particular, low-risk PCa was characterized by about the same value of MD but by many different values of K (Fig 6a). This could suggest that K discriminates further differences in low-GG tissue, not detectable by conventional DTI analysis.

Bourne et al. (43) underlined that stroma is a prostate compartment where microanisotropic diffusion occurs and Lawrence et al. (44) showed that stroma significantly decreases in PCa. Thus, in principle, tissue anisotropy could be a marker for tumor development. Therefore, in this study, for the first

time, KFA was estimated in benign and PCa tissue. Hansen and Jespersen (36) investigated KFA and FA in brain as a function of tissue complexity through simulations. They demonstrated that KFA can reveal tissue anisotropic complexity when FA fails, providing a different image contrast and additional information on tissue composition. However, the estimation of FA in prostate tissue generated contrasting results. Xu et al. (15) observed no significant FA differences between cancerous and benign tissue with both in vivo and ex vivo experiments; conversely, other authors (45) found FA to be higher in PCa and strongly correlated with GS, while Uribe et al. (46) found a weak correlation. In this study, we tested the possibility that KFA overcomes FA limitations. We found that KFA was able to discriminate PCa from benign tissue, and ROC analysis showed KFA to have a better performance than FA (AUC $[KFA_{p25}] = 0.67$, AUC $[FA_{p25}] = 0.55$), but neither KFA nor FA were correlated with GG. Considering that KFA and FA appeared uncorrelated in high-risk PCa and moderately correlated in low-GG and in benign tissue (Fig 6c and Table 4), these results suggested that KFA could furnish unexplored characteristics of prostate cancerous tissue. However, more studies should be addressed to evaluate KFA in prostate PCa at different Gleason.

One of the limits of this work was the restricted patients' cohort, as well as the in-homogeneous distribution of specimens with different GG. Another limitation lies in the fact that we used TRUS-MRI fusion biopsy as a reference standard. This technique is known to be prone to underestimation of tumors grades, with respect to prostatectomy (47).

Finally, since we acquired DWI using six diffusion gradient directions, we could not calculate the kurtosis tensor, whose estimate needs at least 15 gradient directions (17). Therefore, we measured the apparent kurtosis metrics, which is not rotationally invariant. Further studies employing 15 gradients directions are warranted, with the expectation to obtain a better estimate of both FA and KFA (36) and to improve the diagnostic performances of these parameters.

In conclusion, DKI metrics in prostate tissues provided independent and complementary information to that acquired with DTI metrics, especially in low-grade PCa. Therefore, the combination of these two techniques is able to comprehensively characterize the complex mechanisms underlining PCa-related changes better than conventional diffusion techniques alone. The DWI protocol for apparent kurtosis estimation presented here provided an accurate tumor grades classification in a short scanning time; therefore, it would be potentially feasible for clinical applications.

With respect to conventional diffusion maps, K maps highlighted differences between low- and high-grade PCa and provided images with different normal/cancer tissue contrast that could be helpful to identify smaller lesions. Furthermore, DKI yielded a better diagnostic accuracy in PCa stratification, suggesting that DKI is more sensitive to tissue microchanges occurring with tumor progression compared to DTI.

REFERENCES

1. Torre LA, Bray F, Siegel RL, et al. Global cancer statistics, 2012. CA Cancer J Clin 2015; 65:87–108.
2. Rosenkrantz AB, Hindman N, Lim RP, et al. Diffusion weighted imaging of the prostate: comparison of b1000 and b2000 image sets for index lesion detection. J Magn Reson Imaging 2013; 38:694–700.
3. Gurses B, Tasdelen N, Yencilek F, et al. Diagnostic utility of DTI in prostate cancer. Eur J Radiol 2011; 79:172–176.
4. Li L, Margolis DJ, Deng M, et al. Correlation of Gleason scores with magnetic resonance diffusion tensor imaging in peripheral zone prostate cancer. J Magn Reson Imaging 2015; 42:460–467.
5. Nezzo M, Di Trani MG, Caporale A, et al. Mean diffusivity discriminates between prostate cancer with grade group 1 & 2 and grade groups equal to or greater than 3. Eur J Radiol 2016; 85:1794–1801.
6. Weinreb JC, Barentsz JO, Choyke PL, et al. PI-RADS prostate imaging - reporting and data system: 2015, version 2. Eur Urol 2016; 69:16–40.
7. Steiger P, Thoeny HC. Prostate MRI based on PI-RADS version 2: how we review and report. Cancer Imaging 2016; 16:9.
8. Scheenen TW, Rosenkrantz AB, Haider MA, et al. Multiparametric magnetic resonance imaging in prostate cancer management: current status and future perspectives. Invest Radiol 2015; 50:594–600.
9. Murphy G, Haider M, Ghai S, et al. The expanding role of MRI in prostate cancer. AJR Am J Roentgenol 2013; 201:1229–1238.
10. Walsh PC, DeWeese TL, Eisenberger MA. Clinical practice. Localized prostate cancer. N Engl J Med 2007; 357:2696–2705.
11. Daneshgari F, Taylor GD, Miller GJ, et al. Computer simulation of the probability of detecting low volume carcinoma of the prostate with six random systematic core biopsies. Urology 1995; 45:604–609.
12. Fine SW, Epstein JI. A contemporary study correlating prostate needle biopsy and radical prostatectomy Gleason score. J. Urol 2008; 179:1335–1339.
13. Ahmed HU, Akin O, Coleman JA, et al. Transatlantic consensus group on active surveillance and focal therapy for prostate cancer. BJU Int 2012; 109:1636–1647.
14. Gleason D. Histologic grading and clinical staging of carcinoma of the prostate. In: Tannenbaum M, ed. Urologic pathology: the prostate, Philadelphia, PA: Lea & Febiger; 1977; 171–198.
15. Xu J, Humphrey PA, Kibel AS, et al. Magnetic resonance diffusion characteristics of histologically defined prostate cancer in humans. Magn Reson Med 2009; 61:842–850.
16. Ning P, Shi D, Sonn GA, et al. The impact of computed high b-value images on the diagnostic accuracy of DWI for prostate cancer: a receiver operating characteristics analysis. Sci Rep 2018; 8:3409.
17. Jensen JH, Helpern JA, Ramani A, et al. Diffusional kurtosis imaging: the quantification of non-Gaussian water diffusion by means of magnetic resonance imaging. Magn Reson Med 2005; 53:1432–1440.
18. Jansen JF, Stambuk HE, Koutcher JA, et al. Non-Gaussian analysis of diffusion-weighted MR imaging in head and neck squamous cell carcinoma: a feasibility study. AJNR Am J Neuroradiol 2010; 31:741–748.
19. Palombo M, Gentili S, Bozzali M, et al. New insight into the contrast in diffusional kurtosis images: does it depend on magnetic susceptibility? Magn Reson Med 2015; 75:2015–2024.
20. De Santis S, Gabrielli A, Palombo M, et al. Non-Gaussian diffusion imaging: a brief practical review. Magn Reson Imaging 2011; 29:1410–1416.
21. Wang Q, Li H, Yan X, et al. Histogram analysis of diffusion kurtosis magnetic resonance imaging in differentiation of pathologic Gleason grade of prostate cancer. Urol Oncol 2015; 33:337.e15–337.e24.
22. Donati OF, Mazaheri Y, Afaq A, et al. Prostate cancer aggressiveness: assessment with whole-lesion histogram analysis of the apparent diffusion coefficient. Radiology 2014; 271:143–152.
23. Rosenkrantz AB, Sigmund EE, Johnson G, et al. Prostate cancer: feasibility and preliminary experience of a diffusional kurtosis model for detection and assessment of aggressiveness of peripheral zone cancer. Radiology 2012; 264:126–135.
24. Suo S, Chen X, Wu L, et al. Non-Gaussian water diffusion kurtosis imaging of prostate cancer. Magn Reson Imaging 2014; 32:421–427.
25. Roethke MC, Kuder TA, Kuru TH, et al. Evaluation of diffusion kurtosis imaging versus standard diffusion imaging for detection and grading of peripheral zone prostate cancer. Invest Radiol 2015; 50:483–489.
26. Toivonen J, Merisaari H, Pesola M, et al. Mathematical models for diffusion-weighted imaging of prostate cancer using b values up to 2000 s/mm2: correlation with Gleason score and repeatability of region of interest analysis. Magn Reson Med 74:1116–1124.

27. Tamura C, Shinmoto H, Soga S, et al. Diffusion kurtosis imaging study of prostate cancer: preliminary findings. J Magn Reson Imaging 2014; 40:723–729.
28. Pierorazio PM, Walsh PC, Partin AW, et al. Prognostic Gleason grade grouping: data based on the modified Gleason scoring system. BJU Int 2013; 111:753–760.
29. Epstein JI, Egevad L, Amin MB, et al. The 2014 International Society of Urological Pathology (ISUP) Consensus Conference on Gleason Grading of Prostatic Carcinoma: definition of grading patterns and proposal for a new grading system. Am J Surg Pathol 2016; 40:244–252.
30. Chan TY, Partin AW, Walsh PC, et al. Prognostic significance of Gleason score 3+4 versus Gleason score 4+3 tumor at radical prostatectomy. Urology 2000; 56:823–827.
31. Kang DE, Fitzsimons NJ, Presti Jr JC, et al. SEARCH Database Study Group. Risk stratification of men with Gleason score 7 to 10 tumors by primary and secondary Gleason score: results from the SEARCH database. Urology 2007; 70:277–282.
32. Jenkinson M, Beckmann CF, Behrens TE, et al. FSL. NeuroImage 2012; 62:782–790.
33. Kiselev VG. Fundamentals of diffusion MRI physics. NMR Biomed 2017; 30:e3602.
34. Basser PJ, Mattiello J, LeBihan D. Estimation of the effective self-diffusion tensor from the NMR spin echo. J Magn Reson 1994; 103:247–254.
35. Kiselev VG. The cumulant expansion: an overarching mathematical framework for understanding diffusion NMR. In: Jones DK, ed. Diffusion MRI: theory, methods, and applications, Oxford: Oxford University Press; 2010; 152–168.
36. Hansen B, Jespersen SN. Kurtosis fractional anisotropy, its contrast and estimation by proxy. Sci Rep 2016; 6:23999. doi:10.1038/srep23999.
37. Hempel JM, Schittenhelm J, Brendle C, et al. Histogram analysis of diffusion kurtosis imaging estimates for in vivo assessment of 2016 WHO glioma grades: a cross-sectional observational study. Eur J Radiol 2017; 95:202–211.
38. Gibbons JD, Chakraborti S. Nonparametric statistical inference. 5th ed. Boca Raton, FL: Chapman & Hall/CRC Press, Taylor & Francis Group, 2011.
39. Jones DK, Basser PJ. "Squashing peanuts and smashing pumpkins": how noise distorts diffusion-weighted MR data. Magn Reson Med 2004; 52:979–993.
40. Johansson A, Rudolfsson S, Hammarsten P, et al. Mast cells are novel independent prognostic markers in prostate cancer and represent a target for therapy. Am J Pathol 2010; 177:1031–1041.
41. Roma AA, Magi-Galluzzi C, Kral MA, et al. Peritumoral lymphatic invasion is associated with regional lymph node metastases in prostate adenocarcinoma. Mod Pathol 2006; 19:392–398.
42. Humphrey PA. Gleason grading and prognostic factors in carcinoma of the prostate. Mod Pathol 2004; 17:292–306.
43. Bourne RM, Kurniawan N, Cowin G, et al. Microscopic diffusion anisotropy in formalin fixed prostate tissue: preliminary findings. Magn Reson Med 2012; 68:1943–1948.
44. Lawrence EM, Warren AY, Priest AN, et al. Evaluating prostate cancer using fractional tissue composition of radical prostatectomy specimens and pre-operative diffusional kurtosis magnetic resonance imaging. PLoS One 2016; 11:e0159652.
45. Tian W, Zhang J, Tian F, et al. Correlation of diffusion tensor imaging parameters and Gleason scores of prostate cancer. Exp Ther Med 2018; 15:351–356.
46. Uribe CF, Jones EC, Chang SD, et al. In vivo 3T and ex vivo 7T diffusion tensor imaging of prostate cancer: correlation with histology. Magn Reson Imaging 2015; 33:577–583.
47. Lanz C, Cornud F, Beuvon F, et al. Gleason score determination with transrectal ultrasound-magnetic resonance imaging fusion guided prostate biopsies—are we gaining in accuracy? J Urol 2016; 195:88–93.